The impact of weather pattern and related transport processes on aviation's contribution to ozone and methane concentrations from NO_x emissions

Simon Rosanka[1,a], Christine Frömming[2], and Volker Grewe[1,2]

[1]Delft University of Technology, Faculty of Aerospace Engineering, Section Aircraft Noise Climate Effects, Delft, The Netherlands
[2]Deutsches Zentrum für Luft- und Raumfahrt, Institute of Atmospheric Physics, Oberpfaffenhofen, Germany
[a]now at: Forschungszentrum Jülich GmbH, Institute of Energy and Climate Research, IEK-8: Troposphere, Jülich, Germany

Correspondence: Volker Grewe (volker.grewe@dlr.de)

Abstract. Aviation attributed climate impact depends on a combination of composition changes in trace gases due to emissions of carbon dioxide (CO_2) and non-CO_2 species. Nitrogen oxides (NO_x = NO + NO_2) emissions induce an increase in ozone (O_3) and a depletion of methane (CH_4) leading to a climate warming and a cooling, respectively. In comparison to CO_2, non-CO_2 contributions to the atmospheric composition are short lived and are thus characterised by a high spatial and temporal variability. In this study, we investigate the influence of weather patterns and their related transport processes on composition changes caused by aviation attributed NO_x emissions. This is achieved by using the atmospheric chemistry model EMAC (ECHAM/MESSy). Representative weather situations were simulated in which unit NO_x emissions are initialised in specific air parcels at typical flight altitudes over the North Atlantic flight sector. By explicitly calculating contributions to the O_3 and CH_4 concentrations induced by these emissions, interactions between trace gas composition changes and weather conditions along the trajectory of each air parcel are investigated. Previous studies showed a clear correlation between the prevailing weather situation at the time when the NO_x emission occurs and the climate impact of that NO_x emission. Here, we show that the aviation NO_x contribution to ozone is characterised by the time and magnitude of its maximum and demonstrate that a high O_3 maximum is only possible if the maximum occurs early after the emission. Early maxima occur only if the air parcel, in which the NO_x emission occurred, is transported to lower altitudes, where the chemical activity is high. This downward transport is caused by subsidence in high pressure systems. A high ozone magnitude only occurs if the air parcel is transported downward into a region in which the ozone production is efficient. This efficiency is limited by atmospheric NO_x and HO_x concentrations during summer and winter, respectively. We show that a large CH_4 depletion is only possible if a strong formation of O_3 occurs due to the NO_x emission and if high atmospheric H_2O concentrations are present along the air parcel's trajectory. Only air parcels which are transported into tropical areas, due to high pressure systems, experience high concentrations of H_2O and thus a large CH_4 depletion. Thus, the controlling factor to identify the climate impact from aviation NO_x emissions are transport processes. Avoiding climate sensitive areas by re-routing aircraft flight tracks is currently computationally not feasible due to the long chemical simulations needed. The findings in this study comprises a step towards

a climate impact assessment of individual flights, here with the contribution of aviation NO_x emissions to climate change, ultimately enabling routings with a lower climate impact by avoiding climate-sensitive regions.

1 Introduction

The importance of anthropogenic climate change has been well established since years (Shine et al., 1990) and it is well known that air traffic contributes substantially to the total anthropogenic climate change (Lee et al., 2009; Brasseur et al., 2016; Grewe et al., 2017a). A major fraction of its contribution comes from non-CO_2 emissions which lead to changes in greenhouse gas concentrations as well as contrail and contrail-cirrus formation in the atmosphere (Kärcher, 2018). The climate impact of CO_2 is mainly characterised by the emissions strength, due to its long lifetime. However, non-CO_2 effects are known to be characterised by a high spatial and temporal variability. This implies that the total contribution to concentrations of non-CO_2 emissions is not only influenced by the emissions strength but also by the time and location of the emission itself.

Nitrogen oxides (NO_x = NO + NO_2), emitted in the upper troposphere, lead to a formation of ozone (O_3) following a catalytic reaction. NO reacts with HO_2 forming NO_2. Via photodissociation, NO_2 forms $O(^3P)$ leading to the formation of O_3.

$$HO_2 + NO \rightarrow OH + NO_2 \quad \text{(R1)}$$

$$NO_2 + h\nu(\lambda \leq 410nm) \rightarrow NO + O(^3P) \quad \text{(R2)}$$

$$O(^3P) + O_2 + M \rightarrow O_3 + M \quad \text{(R3)}$$

The additionally formed OH leads to an oxidation of CH_4:

$$CH_4 + OH \rightarrow CH_3 + H_2O \quad \text{(R4)}$$

Additional concentration changes in ozone are introduced by changes to the precursor methane, known as primary mode ozone (PMO) (Wild et al., 2001). Earlier studies already identified that the climate impact resulting from aviation attributed NO_x emissions varies strongly within the atmosphere. In general, the increase in O_3 has a warming effect whereas the depletion of CH_4 leads to cooling effect. The warming caused by O_3 out weights the cooling via CH_4 leading to an overall warming due to aviation attributed NO_x emissions (Lee et al., 2009; Grewe et al., 2019). Köhler et al. (2013) showed that the climate impact is larger for emissions occurring in lower than in higher latitudes. A larger climate impact also occurs in regions with low aviation activity (such as in low altitudes and latitudes) for the same amount of NO_x. Both can be explained by higher incoming solar radiation and lower background NO_x concentrations in those regions compared to higher latitudes. A similar impact was identified by Stevenson and Derwent (2009). The general lower background NO_x concentration in the Southern Hemisphere (SH) compared to the Northern Hemisphere (NH) also explains the inter-hemispheric discrepancy of the resulting climate impact from NO_x emissions. In the SH the climate impact from the same amount of NO_x is generally larger. Köhler et al. (2008) identified that the emission altitude strongly influences the resulting climate impact, which is generally larger for emissions at high altitudes. Frömming et al. (2012) demonstrated that the overall climate impact can be reduced by adapting

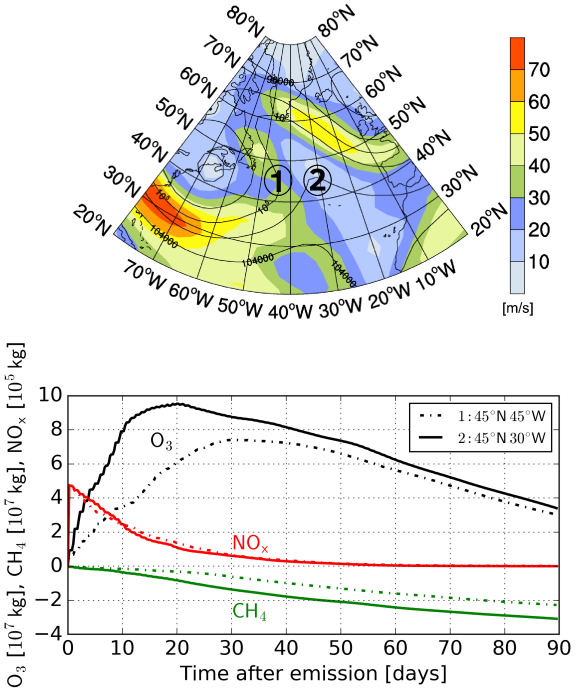

Figure 1. Weather conditions at time of emission (top) represented by geopotential height (black contours in gpm) and wind velocities (see colorbar, in $\mathrm{m\,s^{-1}}$) and the composition change in O_3 and CH_4 induced by the emitted NO_x at two emission locations (bottom).

flight altitudes, suggesting a possible mitigation strategy. The season in which the emission occurs influences the resulting climate impact in addition to the emission location. Gilmore et al. (2013) identified that during summer the production of O_3 is about 50 % higher in summer and 40 % lower in winter, when compared to the annual mean. Changes in CH_4 lifetime compensate parts of this higher O_3 production, leading only to a 10 % higher climate impact. In winter, the resulting climate impact is about 10 % lower. Grewe et al. (2017a) and Frömming et al. (2020) demonstrated that the total change in ozone is larger if the NO_x emission occurred within a high pressure ridge compared to emissions occurring west of this blocking condition.

Figure 1 shows the "typical" temporal development of O_3 and CH_4 due to an aviation attributed NO_x emission for two emission locations next to each other (45°N 45°W and 45°N 30°W), representative for the examples presented in Grewe et al. (2017a) and Frömming et al. (2020). In exact, one emission region is within and the other one is west of a high pressure ridge (see top panel in Fig. 1). NO_x is reduced almost exponentially and washed out after about a month. While the emitted NO_x decreases, the O_3 concentration increases due to the described production processes (Reaction R1 - R3). When the NO_x mixing ratio is below a certain level, only little O_3 is produced and loss terms dominate the O_3 chemistry leading to a continuous decrease in the formed O_3. At the same time, the additional O_3 and NO_x form OH leading to a depletion of CH_4 (Reaction R4). After all NO_x and O_3 is lost, the negative CH_4 anomaly starts to decay and will later reach its original values

Table 1. The integrated O_3 and CH_4 contribution to atmospheric concentration for both locations given in Fig. 1. Additionally, the resulting climate impact for both locations is given. For further details on the climate impact see Frömming et al. (2020). Integrals are given in $\mathrm{kg\ days}$ and Climate-Cost-Functions (CCF) are given in $\mathrm{K\ kg(N)^{-1}}$.

-	45°N 45°W	45°N 30 °W
Integral O_3	469.6×10^7	600.3×10^7
Integral CH_4	-99.9×10^7	-158.5×10^7
CCF O_3	1.65×10^{-12}	2.31×10^{-12}
CCF CH_4	-9.19×10^{-13}	-9.56×10^{-13}
CCF PMO	-2.67×10^{-13}	-2.78×10^{-13}

(not seen in Figure 1). For these two emission regions, the resulting O_3 gain differs, with the one emitted in the high pressure system having an earlier O_3 maximum with a higher magnitude. In contrast, the CH_4 depletion is only characterised by a varying magnitude. This large variability in the NO_x-O_3-CH_4 relation, induced by the same NO_x emission, is also presented in Fig. 9 of Grewe et al. (2014). The question remains if the different resulting characteristics for both emission locations given in Fig. 1 can be explained by the the different weather conditions experienced by each air parcel.

Within the present study, we investigate the impact of weather situations on changes in ozone and methane concentrations induced by NO_x emissions in the upper troposphere, emitted over the North Atlantic flight sector. In general, one tends to analyse the integrated O_3 change or the integrated radiative forcing due to these changes in O_3. Table 1 gives the integrated O_3 and CH_4 for both regions (see Fig. 1). Additionally, the so called Climate Change Functions (CCFs), a measure on how the Earth surface temperature will change due to a locally restricted NO_x emission (for more details see Grewe et al. (2014) and Frömming et al. (2020)), is given. It becomes obvious that an earlier and larger O_3 change leads to a higher integrated O_3 and a higher climate impact. Analysing the integrated O_3 and CH_4 is not feasible when analysing the influence of weather conditions on the induced composition changes due to aviation attributed NO_x emissions. Comparing varying weather conditions to a single data point (e.g. the integrated O_3) is difficult, due to the chaotic nature of weather conditions. Typical characteristics of the temporal development of O_3 and CH_4 are more suitable for this analysis since it is expected that they are directly influenced by varying weather conditions. Therefore, special focus in this study is on how weather conditions influence the time when the O_3 maximum occurs, the total O_3 gained as well as the total CH_4 depleted. Our findings are additionally analysed with respect to inter-seasonal variability. This is achieved by using the results of simulations performed in the European project REACT4C (Reducing Emissions from Aviation by Changing Trajectories for the benefit of Climate, https://www.react4c.eu/ (Matthes, 2011)). The modelling approach of REACT4C as well as the methodology used in this study is elaborated in Section 2. Afterwards all findings of this study will be presented (Section 3). In Section 4, uncertainties and findings of this study will be discussed. Possible implementation strategies are presented in the conclusion (Section 5).

2 Methodology

Our analysis of the general concept of REACT4C as well as the modelling approach used will be elaborated first, to understand how the impacts of NO_x emissions on O_3 and CH_4 were simulated. The idea of the project is presented by Matthes (2011) and Matthes et al. (2012). A complete description of the modelling approach used is given by Grewe et al. (2014). Afterwards, a detailed description of the steps taken within the analysis of this work is presented.

2.1 REACT4C

REACT4C investigated the feasibility of adapting flight routes and flight altitudes to minimise the climate impact of aviation and estimate the global effect of such air traffic management (ATM) measures (Grewe et al., 2014). In this particular study, this mitigation option was tested over the North Atlantic region. The general steps in this modelling approach were as follows: (1) select representative weather patterns, (2) define time-regions, (3) model atmospheric contributions for additional emissions in these time-regions, (4) calculate the adjusted radiative forcing (RF), (5) calculate the climate change function (CCF) for each emission species and induced cloudiness, (6) optimize aircraft trajectories, based on the CCF results, by using an air traffic simulation system (System for traffic Assignment and Analysis at a Macroscopic level, SAAM) which is coupled to an emission tool (Advanced Emission Model, AEM), and (7) calculate the resulting operation costs and the resulting climate impact reduction. For the present study, only step one to three are important and will be further elaborated.

Irvine et al. (2013) identified, that by simulating frequently occurring weather situations within a season, the global seasonal impact can be estimated. They analysed meteorological reanalysis data for 21 years for summer and winter. This reanalysis leads to three distinct summer (SP1-3) and five winter patterns (WP1-5). The different weather patterns mainly vary in their location, orientation and strength of the jet stream and the phase of the North Atlantic Oscillation and the Arctic Oscillation, two distinct teleconnection patterns. A graphical representation of each defined weather pattern is given by Irvine et al. (2013, Fig. 7 and Fig. 8 for winter and summer, respectively) and the actual weather situations simulated in REACT4C are presented in Frömming et al. (2020). Due to the lower variability of the jet stream in summer, only three distinct weather situations were determined. The summer pattern occur 19 (SP1), 55 (SP2) and 18 (SP3) and the winter pattern 17 (WP1 & WP2), 15 (WP3 & WP4) and 26 (WP5) times per season in the reanalysis data (Irvine et al., 2013). Analogously, REACT4C simulated eight distinct model days, each representing one of these weather patterns.

To calculate the climate change functions, a time-region grid was defined in the North Atlantic region for seven latitudes (between 30°N to 80°N) and six longitudes (between 80°W to 0°W) over 4 different pressure levels (200, 250, 300 and 400 hPa) to account for different flight levels. At each time-region grid point, unit emissions of CO_2, NO_x and H_2O are initialised on 50 trajectories at 6, 12 and 18 UTC. However, Grewe et al. (2014) found that the results show only minor sensitivity with respect to the temporal resolution. Therefore, only 12 UTC is considered in this study. The 50 trajectories are randomly located in the respective model grid box in which the specific time-region grid point is located. At each time-region grid point, 5×10^5 kg of NO (equals 2.33×10^5 kg(N)) are emitted, which is then equally distributed onto the trajectories (Grewe et al., 2014).

2.2 Base model description

The ECHAM/MESSy Atmospheric Chemistry (EMAC) model is a numerical chemistry and climate simulation system that includes sub-models describing tropospheric and middle atmosphere processes and their interaction with oceans, land and human influences (Jöckel et al., 2010). It uses the second version of the Modular Earth Submodel System (MESSy2) to link multi-institutional computer codes. The core atmospheric model is the 5th generation European Centre Hamburg general circulation model (ECHAM5, Roeckner et al. (2003)). For the present study we applied EMAC (ECHAM5 version 5.3.02, MESSy version 2.52.0) in the T42L41-resolution, i.e. with a spherical truncation of T42 (corresponding to a quadratic Gaussian grid of approximately 2.8 by 2.8 degrees in latitude and longitude) with 41 vertical hybrid pressure levels up to 5 hPa.

The applied model setup comprised multiple MESSy submodules important for the performed simulations. Each of the tracers (i.e. NO_x and H_2O) is emitted in an air parcel by the submodel TREXP (Tracer Release EXperiments from Point sources). The air parcel is then advected by the submodel ATTILA (Atmospheric Tracer Transport In a LAgrangian model) (Reithmeier and Sausen, 2002) using the wind field from EMAC. In addition to the 50 air parcels with tracer loading starting at each time-region, empty background air parcels are modelled in the northern hemisphere to allow for additional mixing, which in total yields about 169000 air parcels. The air parcels have a constant mass and the mixing ratio of each species is defined on the parcels centroid. The centroid is assumed to be representative for the whole air parcel and the Lagrangian cells are considered isolated air parcels. While ATTILA is per se non-diffusive, inter-parcel mixing is parameterized by bringing the mass mixing ratio in a parcel closer to the average background mixing ratio, which is the average mixing ratio of all parcels within a grid box. The vertical transport due to subgrid-scale convection in ATTILA is calculated in three steps. First, mapping the ATTILA tracer concentrations from the air parcels to the EMAC grid. Second, calculating the convective mass fluxes similarly as for standard EMAC tracers. Third, mapping the calculated tendencies back to the air parcels. While a gain of tracer mass is distributed evenly among the air parcels in a grid cell, a reduction of tracer mass is calculated according to the mass available. Further details are given in Reithmeier and Sausen (2002).

For each trajectory the contribution of the emission (i.e. NO_x and H_2O) to the atmospheric concentration of CH_4, O_3, HNO_3, H_2O and OH is calculated over a time period of 90 days by using the submodel AIRTRAC (version 1.0, Frömming et al. (2013); see Supplement of Grewe et al. (2014)). The tagging approach used by AIRTRAC was first described by Grewe et al. (2010). In this approach each important chemical reaction is doubled. The first reaction applies to the whole atmosphere (from here onwards referred to as background) and the second one only to the additionally emitted tracer (from here onwards referred to as foreground). The submodel MECCA (Module Efficiently Calculating the Chemistry of the Atmosphere) is used to model the background chemical processes in the troposphere and stratosphere. The chemical mechanism used by MECCA can be grouped into sulfur, non-CH_4 hydrocarbon, basic O_3, CH_4, HO_x and NO_x and halogen chemistry (Sander et al., 2005). AIRTRAC on the other hand calculates the resulting changes due to the additional emitted NO_x in the foreground. AIRTRAC assumes that each concentration change of O_3 due to aviation is attributed to the emitted NO_x, which is consistent with Brasseur et al. (1998). Concentration changes due to additionally emitted NO_x are calculated based on the concentration of all chemical species involved in the general chemical system and the concentrations due to the extra emitted NO_x. The actual

concentration change is then calculated based on the background reaction rate and the fraction of foreground and background concentrations of all reactants (Grewe et al., 2010). In detail, the foreground loss of O_3 ($L^f_{O_3}$) via Reaction R5 is based on the foreground and background concentrations of NO_2 and O_3 (NO^f_2, O^f_3 and NO^b_2, O^b_3 for foreground and background, respectively) and the background loss of O_3 ($L^b_{O_3}$), as given in Equation 1.

$$NO_2 + O_3 \rightarrow NO + 2O_2 \quad \text{(R5)}$$

$$L^f_{O_3} = L^b_{O_3} \times \frac{1}{2}\left(\frac{NO^f_2}{NO^b_2} + \frac{O^f_3}{O^b_3}\right) \quad (1)$$

In total, AIRTRAC calculates the mass development of NO_x, O_3, HNO_3, OH, HO_2 and H_2O by tracking 14 reactions and reaction groups. One group for the production and one for the destruction of O_3 as well as one for the formation of HNO_3. Three and five reactions are tracked for the OH production and destruction, respectively. In addition, three reaction groups for the production and destruction of HO_2 are tracked. Further loss processes like wash-out and deposition are taken into account (Grewe et al., 2014). The results of this mechanism agrees well with earlier studies with respect to the regionally different chemical regimes and the overall effect of aviation emissions (Grewe et al., 2017b, Section 4.3, therein). The tagging mechanism also enables the quantification of methane losses due to the two major reaction pathways, the change in HO_x partitioning towards OH due to a NO_x emission and the production of OH due to an enhanced ozone concentration (Grewe et al., 2017b, Figure 8). Section 4 includes an elaborate discussion on the modelling approach used.

2.3 Analysis performed in this study

Within this study we used the simulation output created by the REACT4C project. As some output variables were not available for all emission locations and weather patterns, not all time regions and weather pattern could be included in the present study. Some of the raw data of WP2 were subject to data loss and not all analyses could be performed with this weather pattern. Therefore, WP2 has been excluded from this analysis. Emissions occurred in a time region grid of 7 latitudes, 6 longitudes and 4 pressure levels at 12 UTC. From originally 1344, 1115 emission locations are analysed. At each emission location all 50 air parcels are taken into account, resulting in 55750 trajectories being analysed. An output resolution of six hours was used by REACT4C over 90 days.

The variables taken into account in this analysis can be categorised into three different groups: (1) background and foreground chemical concentrations, (2) background and foreground chemical reaction rates and (3) general weather information. All foreground variables are present on the tracer grid (trajectory id and time), whereas background data are stored on the original EMAC grid. To simplify our analysis, background data were re-gridded onto the tracer grid. Here it was assumed that all background data within a grid box are valid for each air parcel within this specific EMAC grid box.

Due to the general complexity of the atmospheric chemistry, many variables can potentially influence changes in O_3 and CH_4 concentrations induced by NO_x emissions. Therefore, correlation matrices were used to identify interacting parameters. For these matrices the three most common statistical measures to identify correlations were used (Pearson, Kendall, and Spearman's

rank correlation coefficient). Statistical significance is ensured by using t-, one-way analysis of variance (ANOVA) and Tukey's honest significant difference (HSD) tests.

The long term reduction of ozone due to the induced CH_4 loss (i.e. PMO) occurs far beyond the 90 days simulated by REACT4C. Simulating the effect of PMO explicitly is computationally too expensive for the modelling approach used. In REACT4C, PMO was thus not modelled explicitly. Instead a constant scaling factor of 0.29, based on Dahlmann (2012), was applied to the resulting climate impact of methane (Grewe et al., 2014). The effect of PMO is therefore not considered within in this study and focus will be on the total CH_4 depletion, only.

3 Results

Within this section, the results of this study are described. First, a short analysis of the characteristics of the variability in the O_3 maximum is presented. The influence of transport processes on the time of the O_3 maximum is analysed in Section 3.2. The mechanisms controlling total O_3 gained are investigated in Sec. 3.3. The influence of tropospheric water vapour on total CH_4 depletion is discussed in Section 3.4. These findings are presented for summer and winter. An inter-seasonal variability analysis is performed in Section 3.5.

3.1 Characteristics of the temporal development of O_3

Figure 2 shows the maximum O_3 mixing ratio in relation to the time after emission when the maximum occurs. During winter and summer, high concentration changes are only possible if the O_3 maximum occurs early. In this scope, the O_3 maximum is defined as the maximum mixing ratio after which no further increase of O_3 occurs. Figure 3 shows the "typical" temporal development of O_3 for an early, a mid and a late O_3 maximum. The early maximum is characterised by a high production of O_3 in the first days after emission. The mid and late maximum are dominated by a slower O_3 production. In the case of the late maxima, the extreme slow O_3 production leads to a stretched version of temporal development of the air parcel with the early and mid maximum. As stated in Sec. 1, only the early maximum is characterised by a high O_3 maximum and the magnitude decreases by 1/3 and 2/3 for the mid and late maxima, respectively. The top panel of Fig. 2 gives the frequency of when the maximum occurs for both seasons. About 47.5 % and 72 % of all air parcels reach their O_3 maximum during the first 21 days in winter and summer, respectively. Only a small number of air parcels reach their maximum towards the end of the simulation (winter: 2.5 %, summer: < 1 %). All air parcels with a maximum at the end of the simulation are emitted at higher altitudes (200 or 250 hPa) and high latitudes. During winter, these air parcels stay at high latitudes and do not experience any solar radiation (i.e. solar night). The missing solar radiation dampens the O_3 formation, leading to no distinct O_3 maximum within the 90 simulated days.

3.2 Importance of transport processes on the time of the O_3 maxima

It is well established that the ozone production efficiency depends on the general chemical activity, controlled by weather conditions (i.e. temperature), and the concentration of each reactant. These weather conditions and reactant concentrations

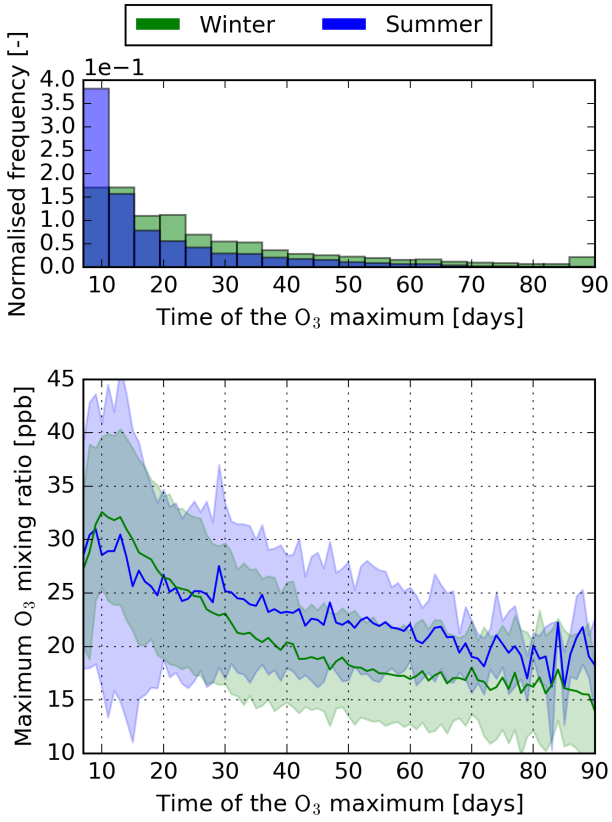

Figure 2. Top: Normalised histogram of when the O_3 maximum is reached after emission. Results are normalised to the total number of air parcel in summer and winter, respectively. Bottom: Mean (solid line) and standard deviation (shaded area) of the maximum O_3 mixing ratio in relation to the time when the O_3 maximum is reached.

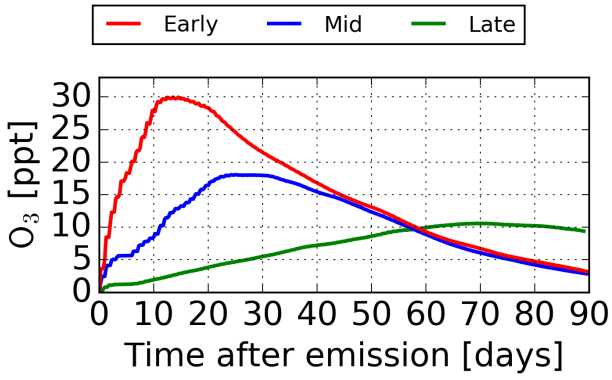

Figure 3. "Typical" temporal development of an early (red), a mid (blue) and a late (green) O_3 maximum.

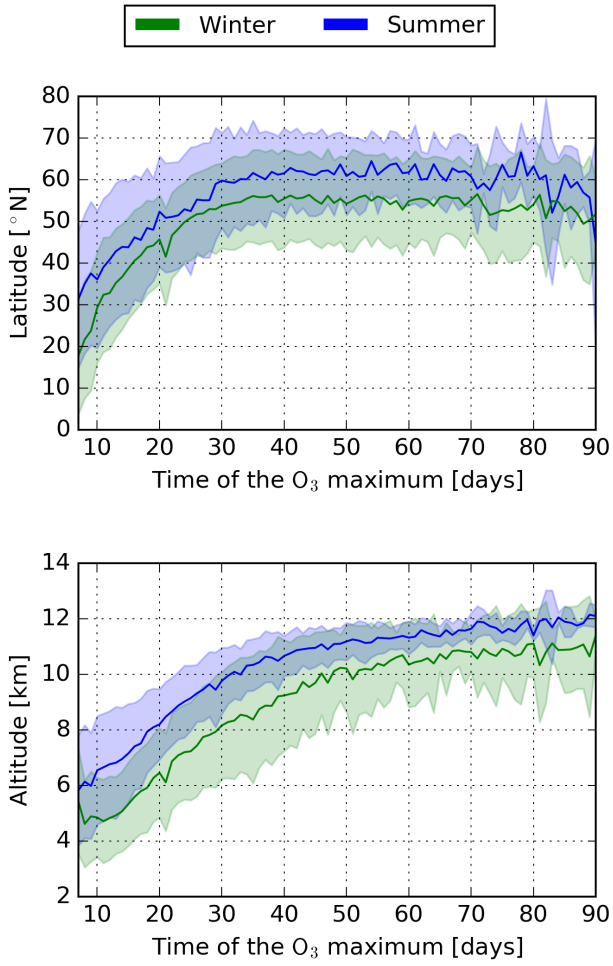

Figure 4. Mean (solid line) and standard deviation (shaded area) of the location of each air parcel within the first seven days after emission in relation to when the maximum O_3 mixing ratio is reached. Top: Latitude. Bottom: Altitude.

differ significantly across the troposphere, such that certain regions have a higher ozone production efficiency. Therefore, the transport into these regions controls the ozone gained. Our analysis shows that air parcels with an early maximum are characterised by a strong downward wind component, whereas late maxima have a weak downward or even an upward vertical wind component (not shown). Therefore, air parcels with an early O_3 maximum are transported to lower altitudes (top panel in Fig. 4) and lower latitudes (bottom of Fig. 4). Air parcels with a late maximum mostly stay at the emission altitude and latitude or are transported to higher altitudes and latitudes. For all winter patterns most maxima occur in a region spanning from 15°N to 35°N at pressure altitudes between 900 to 600 hPa. The maximum region is slightly shifted to higher altitudes for all summer patterns. No maximum occurs at high latitudes during winter due to the absence of solar radiation in the polar region during

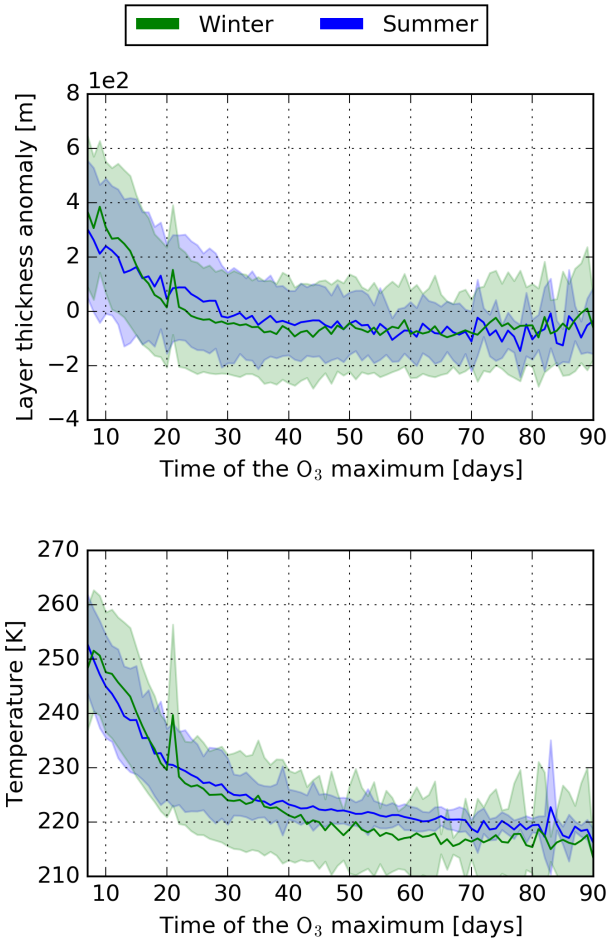

Figure 5. Top: Mean thickness of the 850 - 250 hPa layer. Bottom: Mean dry air temperature. In both cases the relation to the time when the O_3 maximum is reached is given. The seasonal mean is represented by the solid line and the standard deviation as shaded area.

this time period. This indicates that a significant O_3 production, leading to an early O_3 maximum, is only possible if an air parcel is transported to lower altitudes and latitudes.

Tropospheric vertical transport processes have many causes, e.g. temperature differences, incoming solar radiation, as well as latent and sensible heat. Vertical transport occurs in deep convection and conveyor belt events and causes an exchange of trace gases between the upper and the lower troposphere. Figure 5 (top) shows the mean layer thickness anomaly of the 850 to 250 hPa layer. The layer thickness is proportional to the mean virtual temperature of the layer: a higher layer thickness indicates a higher temperature and moisture content. Here, the anomaly is presented for a better comparison of summer and winter, since higher mean virtual temperatures during summer lead to generally higher layer thickness values. The anomaly is obtained by deducting the seasonal mean. Air parcels with an early maximum have a higher mean layer thickness, whereas late maxima are associated with low layer thicknesses. In classical weather analysis, the layer thickness is used to identify

synoptic weather systems. This indicates that in our study early maxima only occur if an air parcel originates or is transported into and stays within a high pressure system. No correlation exists between the time of the maximum and the layer thickness at emission (Spearman rank coefficient of -0.2). Still, air parcels originating within in the core of a high pressure system have generally earlier maxima compared to air parcel which are transported into high pressure systems after emission (not shown). It is well known that subsidence is dominating vertical transport processes within high pressure systems, explaining the strong downward motion of air parcels, characterised by early maxima. Air parcels with late maxima stay within low pressure systems in which upward motion dominates.

3.3 Weather conditions controlling the O_3 production efficiency

Even though early O_3 maxima are characterised by strong vertical downward transport, transport processes do not directly influence chemical processes in the atmosphere. Temperature is known to be a major factor controlling chemical processes in the atmosphere and is generally higher at lower altitudes and latitudes. The bottom panel of Fig. 5 shows the mean dry air temperature along the air parcel trajectory until the O_3 maximum is reached. The mean dry air temperature is higher for air parcels with early O_3 maxima, which is due to the downward and southward transport (leading to higher temperatures) within high pressure systems. These higher temperatures lead to higher background chemical activity (higher background reaction rates) and therefore accelerate foreground chemistry. Higher temperatures and enhanced photochemical activity at higher altitudes during NH summer, explain the tendency of earlier maxima in this season.

From classical chemistry the efficient production of O_3 does not only depend on the higher chemical activity, due to higher temperatures, but also on the concentrations of the reactants involved. In the case of the formation of O_3 due to NO_x, these are NO and HO_2 (Reaction R1). Figure 6 and 7 show how the mixing ratios of NO_x and HO_x ($=OH + HO_2$) relate to the maximum O_3 mixing ratio. Here, NO_x and HO_x are used to account for the rapid cycling of the species within each radical group. For both seasons, only low NO_x concentration will lead to high O_3 contributions. The production of O_3 via Reaction R1 to R3 dominates at low background NO_x concentrations, whereas at high background concentrations NO_2 is eliminated by reacting with OH and HO_2 forming nitric acid (HNO_3) and peroxynitric acid (HNO_4), respectively. From Fig. 7 it becomes evident that a high increase in O_3 is only possible at high HO_x concentrations, since at low HO_2 no O_3 will be formed via Reaction R1.

In the upper troposphere the background NO_x concentration is altitude dependent and generally increases towards the tropopause (not shown). On the other hand, HO_x is high at low altitudes and latitudes and decreases towards the tropopause. Air parcels with a fast downward transport, generally experience lower mean background NO_x concentrations and higher HO_x background concentrations, resulting in a higher O_3 gain. Air parcels which stay close to the tropopause or are even transported into the stratosphere experience a high background NO_x concentrations, leading to a lower O_3 formation, since most NO_x is eliminated by forming HNO_3 and HNO_4. In addition, high background HO_x concentrations dominate in high pressure systems (not shown) explaining why air parcels in high pressure systems have a generally higher O_3 formation.

Summer and winter significantly differ with regard to the correlation of NO_x and HO_x with the O_3 maximum. Summer has a high Spearman rank coefficient for NO_x (ρ = -0.69) but only correlates weakly with HO_x (ρ = 0.40). Winter on the other

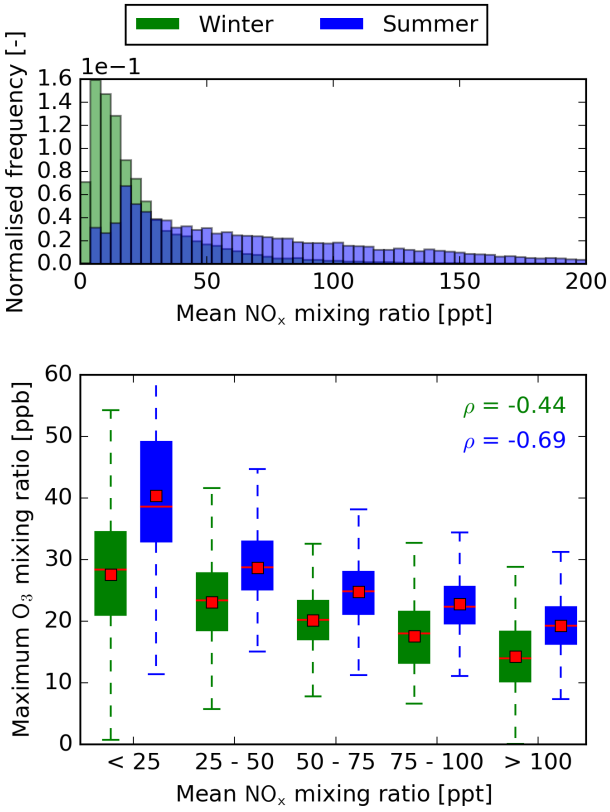

Figure 6. Top: Normalised histogram of the mean NO_x mixing ratio until the O_3 maximum is reached. Results are normalised to the total number of air parcel in summer and winter, respectively. Bottom: Binned box plots showing the relation between the mean NO_x mixing ratio and the magnitude of the O_3 maximum. The median and mean for each box plot are represented by red lines and red boxes, respectively. Additionally, the Spearman rank coefficient is given for summer and winter.

hand correlates well with HO_x (ρ = 0.76) but weakly with NO_x (ρ = -0.44). This difference is explained by varying NO_x and HO_x concentrations in both seasons. The top panel of Fig. 6 and 7 gives the normalised frequency of NO_x and HO_x for both seasons. It becomes evident that winter is characterised by low NO_x and HO_x concentrations, where as summer is dominated by high NO_x and HO_x concentrations. For many air parcels during summer, enough HO_x is present to allow a high formation of O_3, but a higher NO_x concentration limits the formation of O_3 and leads to the formation of HNO_3 and HNO_4. During winter, the low NO_x concentrations theoretically allow for a high O_3 formation but low HO_x concentrations limit the efficient production of O_3.

3.4 Influence of water vapour on the total CH_4 depletion

In comparison to O_3, only the total CH_4 depletion is of interest, due to its longer atmospheric lifetime. A high O_3 concentration leads to a high CH_4 depletion (Spearman rank coefficient of 0.66) since O_3 is a major source of OH, accelerating the depletion

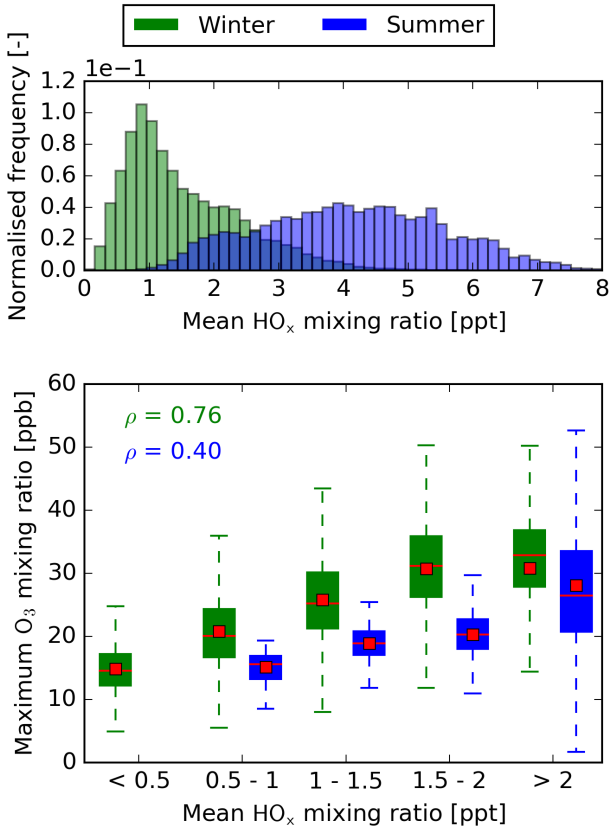

Figure 7. Top: Normalised histogram of the mean HO_x mixing ratio until the O_3 maximum is reached. Results are normalised to the total number of air parcel in summer and winter, respectively. Bottom: Binned box plots showing the relation between the mean HO_x mixing ratio and the magnitude of the O_3 maximum. Please note that during summer HO_x mixing ratios below 0.5 ppt show no statistical significance. Therefore, no box plot is provided in this case. The median and mean for each box plot are represented by red lines and red boxes, respectively. Additionally, the Spearman rank coefficient is given for summer and winter.

of CH_4 (Reaction R4). However, the moderate Spearman rank coefficient indicates that other factors additionally control the CH_4 depletion process. Our results show that a high foreground CH_4 depletion is only possible if the background OH concentration is high. When looking at OH the fast cycling between OH and HO_2 has to be taken into account. Analysing the recycling probability (r) of OH is useful to account for this cycling. Here, we define the recycling probability, following Lelieveld et al. (2002), as:

$$r = 1 - \frac{P}{G} \tag{2}$$

in which P is the primary production of OH via:

$$H_2O + O(^1D) \rightarrow 2OH \tag{R6}$$

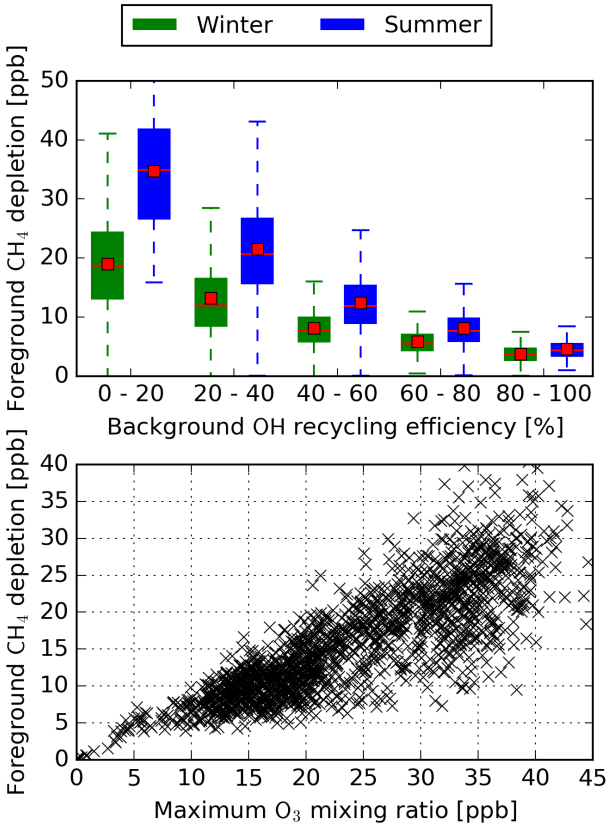

Figure 8. Top: Binned box plots of the OH recycling probability. The median and mean for each box plot are represented by red lines and red boxes, respectively. Bottom: Maximum O_3 mixing ratio vs. maximum CH_4 mixing ratio for recycling probabilities below 20 % for WP1.

and G is the gross OH production additionally considering the secondary production of OH. In general, when r approaches 100 % the formation of OH becomes autocatalytic. When r approaches 0 %, all OH is formed via Reaction R6. Based on a perturbation study, Lelieveld et al. (2002) identified that for recycling probabilities above 60 % the chemical system becomes buffered and that NO_x perturbations in this regime have only little impact on OH. The top of Fig. 8 shows that a high CH_4 depletion is only possible if the recycling probability of background OH is below 60 %. When the major source of OH is from Reaction R6 (r approaches 0 %), the formed OH is not recycled via NO_x, accelerating the depletion of CH_4. The major source of foreground OH is the formed O_3. A high background OH recycling probability does not necessarily mean that foreground O_3 is efficiently produced. The foreground formation of O_3 is limited by background NO_x and HO_x during summer and winter, respectively. Figure 8 (bottom) shows the relation between the total CH_4 depletion and the O_3 magnitude for recycling probabilities below 20 % (most left box-plot in top of Fig. 8). Thus, the possible low O_3 formed limits the CH_4 depletion at low OH recycling probabilities, explaining the high spread in the total CH_4 depletion in that regime. It can thus be concluded that a high depletion of CH_4 is only possible if the major formation of OH is due to Reaction R6.

Table 2. Spearman rank coefficient of all identify relations for each individual weather pattern. All correlation factors related to the time and the maximum O_3 mixing ratio are calculated based on mean values for the time span between emission and the time of the O_3 maximum. The correlation between the total CH_4 depletion and specific humidity is based on the mean between time of emission and the time when the total CH_4 depletion is reached.

Correlation factors		Winter				Summer		
		WP1	WP3	WP4	WP5	SP1	SP2	SP3
Time of O_3 maximum	Vertical wind velocity	-0.67	-0.77	-0.69	-0.61	-0.66	-0.66	-0.57
	850 -250 hPa layer thickness	-0.74	-0.66	-0.61	-0.63	-0.59	-0.63	-0.56
	Mean temperature	-0.78	-0.84	-0.80	-0.79	-0.86	-0.82	-0.81
Maximum O_3 mixing ratio	Mean background NO_x	-0.08	-0.37	-0.43	-0.66	-0.73	-0.76	-0.78
	Mean background HO_2	0.76	0.71	0.71	0.38	0.38	0.21	0.40
Total CH_4 depletion	Specific humidity	0.81	0.82	0.82	0.75	0.74	0.71	0.72

Globally, Lelieveld et al. (2016) estimate that about 30% of the tropospheric OH is produced by Reaction R6. This reaction is limited by the availability of $O(^1D)$, formed from the photolysis of O_3, and H_2O. In this study, the highest CH_4 depletion rate occurs in tropical regions close to the surface (between 0°and 20°N and below 850hPa), which is dominated by hot and humid weather conditions. This region is known to have high HO_x concentrations due to active photochemistry and large OH sources and sinks. Here, the contribution of OH being produced by water vapour is highest (Lelieveld et al., 2016). A strong correlation exists between the average specific humidity along the air parcel trajectory and the total depletion of CH_4 (mean Spearman rank coefficient of 0.77). In particular, air parcels with a low OH recycling probability and thus a high CH_4 depletion are characterised by high specific humidity and high incoming solar radiation. Therefore, a high depletion of CH_4 is only possible if the air parcel is transported towards low altitudes and latitudes. The transport into tropical regions, occurs mainly due to the subsidence in high pressure systems (see Sec. 3.2).

3.5 Inter seasonal variability

Within this study specific weather situations (for graphical representations see Irvine et al. (2013, their Fig. 7 and Fig. 8), and Frömming et al. (2020)) were analysed. Table 2 shows an overview of all correlations analysed within this study for each distinct weather pattern. Vertical transport processes until the O_3 maximum, represented by the vertical wind velocity, correlate reasonably well within both seasons. However, during summer the correlation tends to be lower. Summer pattern 3 has the lowest correlation coefficient and the highest mean downward wind velocity. The pattern is characterised by a high pressure blocking situation, resulting in an overall high layer thickness, resulting in a weaker correlation. It is thus expected that differences in each individual weather situation (i.e. number, location and strength of the high pressure systems) cause the inter-seasonal variability. Additionally, downward transport during summer is less important for air parcels to experience high

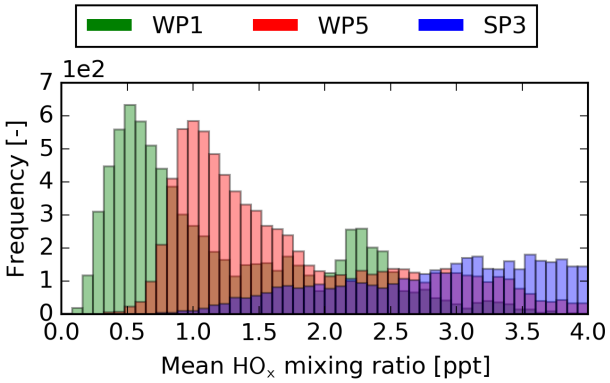

Figure 9. Histogram for the mean HO_x mixing ratio until the O_3 maximum is reached for WP1, WP5 and SP3. Note that mixing ratios above 4 ppt are not shown.

temperatures. This also explains the weaker correlation for the 850 to 250 hPa layer thickness during summer. Still, air parcels which stay in a high pressure region experience earlier maxima during summer.

The mean background concentration of NO_x correlates strongly with the O_3 magnitude for each summer pattern, giving no indication that there is another parameter that controls the total O_3 gain. However, no correlation exists for most winter patterns. This indicated that in winter, when the chemistry is slow at the emission location of mid and higher latitudes, the transport pathway, e.g. towards the tropics, is more important that the chemical background conditions at the time of emission, whereas in summer with active photochemistry the background NO_x concentration plays a role. Only winter pattern five shows a stronger correlation. At the same time, WP5 has a low correlation with HO_x. Figure 9 gives the frequency of the mean background HO_x concentration for WP1, WP5 and SP3. In comparison to WP1, WP5 is characterised by higher HO_x concentrations with most mixing ratios above 1 ppt (WP1 mean: 1.2 ppt, WP5 mean: 1.8 ppt; WP1 median: 0.89 ppt, WP5 median: 1.4 ppt). In general, mixing ratios above 1 ppt allow a high O_3 formation (see Fig. 7). This indicates that for most air parcels in WP5, HO_x is not the only limiting factor. At the same time WP5 is characterised by higher NO_x mixing ratios (WP1 mean: 18.1 ppt, WP5 mean: 31.6 ppt), explaining the higher correlation with NO_x. This indicates that in the case of WP5 the maximum O_3 concentration is limited by a combination of HO_x and NO_x. The chosen example day in EMAC for WP5 occurs at the end February, whereas the other winter patterns are initialised in December or early January. This indicates that HO_x becomes a less limiting factor towards spring. This suggests that our results are only valid for both analysed seasons and further research is necessary to identify the controlling factors in spring and autumn.

Specific humidity is clearly the controlling factor of the total CH_4 depletion for all weather patterns taken into account. Again the correlation is weaker for summer which is due to the generally higher H_2O concentrations. This results in a lower variability in the specific humidity which weakens the correlation analysed. Here, WP5 again behaves like all summer patterns. This indicates that O_3 and CH_4 concentration changes due to emissions in spring are most likely controlled by mechanisms identified for summer.

4 Uncertainties and discussion

Our results indicate a large impact of transport patterns on ozone and methane concentration changes due to aviation NO_x emissions. This is both a highly complex interaction of transport and chemistry, and a relatively small contribution of ozone and methane concentration changes against a large natural variability. Hence, a direct validation of our results is not feasible. However, the main processes, such as transport and chemistry can be evaluated individually - at least in parts. In the following we will discuss some aspects of this interaction and discuss the ability of EMAC to reproduce observations.

An important aspect in our study is the model's transport. Short-lived species which only have a surface source, such as ^{222}Radon (^{222}Rn, radioactive decay half-lifetime of 3.8 d), are frequently used to validate fast vertical transport characteristics. Jöckel et al. (2010) and in more detail Brinkop and Jöckel (2019) showed that the model is able to capture the ^{222}Rn surface concentrations and vertical profiles, indicating that the vertical transport is well represented in EMAC.

The horizontal transport is difficult to evaluate and observed trace gases, which resemble the exchange between mid and high latitudes and the tropics, are not available. However, Orbe et al. (2018) compared transport timescales in various global models, e.g. from northern mid-latitudes to tropics, which differed by 30%. The interhemispheric transport differed by 20%. The authors concluded that vertical transport is a major source of this variability. More research is needed to better constrain models with respect to their tropospheric transport timescales. A more integrated view on the variability of aviation related transport-chemistry interaction is given by a model intercomparison of NO_x concentration differences between a simulation with and without aircraft NO_x emissions (Søvde et al., 2014, see their supplementary material). Here, we concentrate on the winter results to reduce the chemical impact to a minimum. The results clearly show a very similar NO_x change of the 5 models (including EMAC) peaking around 40°N at cruise altitude in winter with a tendency to have a downward and southward transport to the tropics. However, the peak values vary between 55 pptv and 70 pptv.

Chemistry, or more specific, the concentrations of chemically active species is evaluated in detail in Jöckel et al. (2010) and Jöckel et al. (2016). In general, EMAC overestimates the concentrations of tropospheric ozone by 5-10 DU in mid-latitudes and 10-15 DU in the tropics. Carbon monoxide on the other hand is underestimated, though the variability matches well with observations. The tropospheric oxidation capacity is at the lower end of model's estimates, but within the models' uncertainty ranges. Jöckel et al. (2016) speculate that lightning NO_x emissions or stratosphere-to-troposphere exchange might play a role. It is important to note that variations, which are caused by meteorology are in most cases well represented (e.g. Grewe et al., 2017a, their Sec. 3.2).

Ehhalt and Rohrer (1995) already stated that the net-O_3 gain strongly depends in a non-linear manner on the NO_x mixing ratio. This is generally well reproduced in EMAC (Mertens et al., 2018, Figure 5) and even by an EMAC predecessor model (Dahlmann et al., 2011; Grewe et al., 2012, their Figure 4 and Figure 1, respectively). Stevenson et al. (2004) showed the response of ozone and methane to a pulse NO_x emission, which is very similar to our results (Grewe et al., 2014, their Figure 9). Stevenson and Derwent (2009) demonstrated that the NO_x concentration at time of emissions strongly defines the resulting climate impact of O_3. A similar but weaker relation can be found in the current data set (not shown) (Grewe et al., 2014, their Figure 9). For some air parcels the background NO_x concentration is low at time of emission but they are quickly transported

to regions characterised by higher concentrations. These air parcel experience a temporal high O_3 production shortly after emission, due to low NO_x concentrations, but only little total O_3 is formed, due to a high mean background NO_x mixing ratios after emission. This explains the difference between our correlation and the one of Stevenson and Derwent (2009). Another aspect is the question how well the REACT4C concept, to model atmospheric effects of a local emission (Grewe et al., 2014), represents global modelling approaches, such as Søvde et al. (2014) or Grewe et al. (2017b). The approach was developed to gain more insights in aviation effects that can conventionally not be obtained. Hence, there are by definition limitations in answering this question. However, four indications can be given, which support the consistency of the modelling approach. First, the transport scheme is reasonably well established (Brinkop and Jöckel, 2019, and above). Second, the chemical response to a local emission agrees well with earlier findings of Stevenson et al. (2004), who simulated the monthly mean response of ozone and methane to a NO_x pulse and which are very similar to the results from this approach (Grewe et al., 2014, their Fig. 9). Third, the use of a trajectory analysis to interpret either observational data or modelling data is well established (Riede et al., 2009; Cooper et al., 2010). And fourth, a first verification of the resulting global pattern of the atmospheric sensitivity to a local NO_x emission by comparing to sparsly available literature data was promising (Yin et al., 2018). This verification is based on a generalisation of the CCFs by developing algorithms to relate the weather information available at the time of emission to the resulting CCF. These algorithmic CCFs (aCCF, van Manen and Grewe (2019)) allow to predict all weather situations, compared to the limited applicability to a few selected days for the CCFs. An annual climatology of the results from using aCCFs were calculated and compared to conventional approaches (Yin et al., 2018). They conclude: It "shows the variation pattern of the ozone aCCFs matches well with the literature results over the northern hemisphere (the latitude between 30° N and 90°N) and the flight corridor (roughly 9 km to 12 km vertical range)".

From our findings, it can be concluded that not only the atmospheric conditions at the time of emission influences the O_3 gain but rather the region in which the maximum O_3 concentration and the maximum concentration change occur. The findings of Stevenson and Derwent (2009) are also only valid for summer and no winter analysis is provided, making it impossible to directly compare our findings identified in Sec. 3.3 to available literature. However, indirectly, by the use of generalised aCCFs, first findings indicate a reasonably well agreement of the simulated atmospheric response to local NO_x emission.

To conclude, both transport and chemistry processes are crucial for our results. EMAC is in many aspects in line with other model results, but has some biases in the concentration of chemical species. However, the variability of chemical species, such as NO_x and O_3 is better represented than mean values, indicating that the interaction between transport and chemistry is reasonably well simulated. This result should be robust, since our results show a very strong relation between meteorology and the contribution of aviation emission, and since this interaction is in principle well represented in EMAC. However, the strength of the ozone response to a NO_x emission in a high pressure system has an uncertainty, which we hardly can estimate. Based on on the results of the model intercomparison by Søvde et al. (2014), we would expect an uncertainty in the order of 25%.

5 Conclusions

The possibility to reduce aviation's climate impact by avoiding climate sensitive regions, heavily depends on our understanding of the driving influences on induced contributions to the chemical composition of the atmosphere. In this study, we demonstrated the importance of transport processes on locally induced aviation attributed NO_x emission on ozone and methane concentrations over the North Atlantic flight sector. The induced O_3 change is characterised by the time and magnitude of its maximum and high O_3 maxima are only possible if the maximum occurs early. Transport processes like subsidence in high pressure systems lead to early maxima, due to the fast transport into regions with a higher chemical activity. In summer the NO_x-HO_x-relation is limited by background NO_x, whereas in winter the limiting factor are low HO_x concentrations. When an air parcel is transported into regions with high NO_x concentrations in summer, a low change in total ozone occurs, since less ozone is formed in the background. In this case most NO_2 is eliminated by forming nitric acid and peroxynitric acid. During winter low background NO_x concentrations allow for a high O_3 formation but due to generally lower HO_x concentrations no efficient O_3 formation occurs. Air parcels transported quickly towards lower altitudes encounter low NO_x but high HO_x concentrations leading to a higher ozone formation, strengthening the importance of transport processes on the O_3 formation.

The total depletion of methane depends heavily on the background OH concentration. If most OH is formed by its primary formation process, which depends on water vapour, and only little OH is recycled to HO_2, a high depletion of CH_4 occurs. Therefore, the water vapour content which the air parcel experiences along its trajectory defines the total methane depletion. Air parcels transported into lower altitudes and latitudes experience higher water vapour concentrations. Thus, atmospheric transport processes also define the total methane depletion. Additionally, only a high total gain of ozone allows a large methane depletion.

Due to the complexity of the problem, we are not able to validate our results. It would be challenging to design a measurement campaign to proof the contribution of aviation NO_x emissions to ozone and methane. The standard deviation of background concentrations are generally considered to be higher than changes induced by aviation NO_x perturbation, making them hardly detectable (Wauben et al., 1997). Our analysis of the model performance however shows that both transport processes as well as chemical concentrations are reasonably well represented. Our inter seasonal analysis shows that our findings to the importance of background NO_x and HO_x concentrations are only valid for both seasons analysed. Due to the high variability of NO_x and HO_x concentrations in the troposphere, we expect other important factors to control the total ozone gain in other regions, not analysed in this study. Based on the findings of Köhler et al. (2013), we expect our results to be valid for most part of the northern extra-tropics. To conclude, further model studies are necessary to fully quantify how transport processes influence induced changes of ozone and methane concentrations in all seasons as well as other regions of interest.

Mitigating the climate impact from aviation by estimating the climate impact and re-route flight trajectories using the same simulation setup (in resolution, time horizon and chemical mechanism used) as in REACT4C on a day to day basis is currently computationally too expensive and not feasible at the moment. Our results show that transport processes are of most interest when identifying the impact of local NO_x emissions on ozone and methane. Since, purely dynamic simulations without chemistry are computationally less expensive, the insights gained in this work can be used to allow a more feasible approach

by estimating the climate impact based on transport processes and other weather factors (i.e. temperature and humidity). Our results further show that concentration changes of ozone on methane induced by aviation NO_x mainly occur within the first twenty days. Therefore, an alternative approach could be to use shorter simulations to estimate the induced concentration changes and thus reduce computation costs significantly.

Data availability. The data of the REACT4C project used in this work are archived at the German Climate Computing Centre (Deutsches Klimarechenzentrum, DKRZ) and are available on request.

Author contributions. SR and VG designed the analysis and SR carried them out. CF performed the simulations of REACT4C. SR prepared the manuscript with contributions from all co-authors.

Competing interests. The authors declare that they have no conflict of interest.

Acknowledgements. This work was supported by the European Union FP7 Project REACT4C (Reducing Emissions from Aviation by Changing Trajectories for the benefit of Climate: www.react4c.eu/, Grant Agreement Number 233772) and contributes to the DLR project Eco2Fly. Computational resources were made available by the German Climate Computing Center (DKRZ) through support from the German Federal Ministry of Education and Research (BMBF) and by the Leibniz-Rechenzentrum (LRZ). We would like to thank Mariano Mertens from DLR for providing an internal review.

References

Brasseur, G., Cox, R., Hauglustaine, D., Isaksen, I., Lelieveld, J., Lister, D., Sausen, R., Schumann, U., Wahner, A., and Wiesen, P.: European scientific assessment of the atmospheric effects of aircraft emissions, Atmospheric Environment, 32, 2329 – 2418, https://doi.org/https://doi.org/10.1016/S1352-2310(97)00486-X, 1998.

Brasseur, G. P., Gupta, M., Anderson, B. E., Balasubramanian, S., Barrett, S., Duda, D., Fleming, G., Forster, P. M., Fuglestvedt, J., Gettelman, A., Halthore, R. N., Jacob, S. D., Jacobson, M. Z., Khodayari, A., Liou, K.-N., Lund, M. T., Miake-Lye, R. C., Minnis, P., Olsen, S., Penner, J. E., Prinn, R., Schumann, U., Selkirk, H. B., Sokolov, A., Unger, N., Wolfe, P., Wong, H.-W., Wuebbles, D. W., Yi, B., Yang, P., and Zhou, C.: Impact of Aviation on Climate: FAA's Aviation Climate Change Research Initiative (ACCRI) Phase II, Bulletin of the American Meteorological Society, 97, 561–583, https://doi.org/10.1175/BAMS-D-13-00089.1, 2016.

Brinkop, S. and Jöckel, P.: ATTILA 4.0: Lagrangian advective and convective transport of passive tracers within the ECHAM5/MESSy (2.53.0) chemistry–climate model, Geoscientific Model Development, 12, 1991–2008, https://doi.org/10.5194/gmd-12-1991-2019, 2019.

Cooper, O. R., Parrish, D. D., Stohl, A., Trainer, M., Nédélec, P., Thouret, V., Cammas, J. P., Oltmans, S. J., Johnson, B. J., Tarasick, D., Leblanc, T., McDermid, I. S., Jaffe, D., Gao, R., Stith, J., Ryerson, T., Aikin, K., Campos, T., Weinheimer, A., and Avery, M. A.: Increasing springtime ozone mixing ratios in the free troposphere over western North America, Nature, 463, 344–348, https://doi.org/10.1038/nature08708, https://doi.org/10.1038/nature08708, 2010.

Dahlmann, K.: Eine Methode zur effizienten Bewertung von Maßnahmen zur Klimaoptimierung des Luftverkehrs, phdthesis, Ludwig Maximilians Universität, 2012.

Dahlmann, K., Grewe, V., Ponater, M., and Matthes, S.: Quantifying the contributions of individual NO_x sources to the trend in ozone radiative forcing, Atmospheric Environment, 45, 2860 – 2868, https://doi.org/https://doi.org/10.1016/j.atmosenv.2011.02.071, 2011.

Ehhalt, D. and Rohrer, F.: The impact of commercial aircraft on tropospheric ozone, Special Publication-Royal Society of Chemistry, 170, 105–120, 1995.

Frömming, C., Grewe, V., Brinkop, S., and Jöckel, P.: Documentation of the EMAC submodels AIRTRAC 1.0 and CONTRAIL 1.0, supplement of Grewe et al. (2014), 2013.

Frömming, C., Ponater, M., Dahlmann, K., Grewe, V., Lee, D. S., and Sausen, R.: Aviation-induced radiative forcing and surface temperature change in dependency of the emission altitude, Journal of Geophysical Research: Atmospheres, 117, https://doi.org/10.1029/2012JD018204, 2012.

Frömming, C., Grewe, V., Brinkop, S., Jöckel, P., Haslerud, A. S., Rosanka, S., van Manen, J., and Matthes, S.: Influence of the actual weather situation on aviation climate effects: The REACT4C Climate Change Functions (submitted to Atmospheric Chemistry and Physics), ACPD, 2020.

Gilmore, C. K., Barrett, S. R. H., Koo, J., and Wang, Q.: Temporal and spatial variability in the aviation NO_x-related O_3 impact, Environmental Research Letters, 8, 034 027, https://doi.org/10.1088/1748-9326/8/3/034027, 2013.

Grewe, V., Tsati, E., and Hoor, P.: On the attribution of contributions of atmospheric trace gases to emissions in atmospheric model applications, Geoscientific Model Development, 3, 487–499, https://doi.org/10.5194/gmd-3-487-2010, 2010.

Grewe, V., Dahlmann, K., Matthes, S., and Steinbrecht, W.: Attributing ozone to NO_x emissions: Implications for climate mitigation measures, Atmospheric Environment, 59, 102 – 107, https://doi.org/https://doi.org/10.1016/j.atmosenv.2012.05.002, 2012.

Grewe, V., Frömming, C., Matthes, S., Brinkop, S., Ponater, M., Dietmüller, S., Jöckel, P., Garny, H., Tsati, E., Dahlmann, K., Søvde, O. A., Fuglestvedt, J., Berntsen, T. K., Shine, K. P., Irvine, E. A., Champougny, T., and Hullah, P.: Aircraft routing with minimal climate impact: the REACT4C climate cost function modelling approach (V1.0), Geoscientific Model Development, 7, 175–201, https://doi.org/10.5194/gmd-7-175-2014, 2014.

Grewe, V., Dahlmann, K., Flink, J., Frömming, C., Ghosh, R., Gierens, K., Heller, R., Hendricks, J., Jöckel, P., Kaufmann, S., Kölker, K., Linke, F., Luchkova, T., Lührs, B., Van Manen, J., Matthes, S., Minikin, A., Niklaß, M., Plohr, M., Righi, M., Rosanka, S., Schmitt, A., Schumann, U., Terekhov, I., Unterstrasser, S., Vázquez-Navarro, M., Voigt, C., Wicke, K., Yamashita, H., Zahn, A., and Ziereis, H.: Mitigating the Climate Impact from Aviation: Achievements and Results of the DLR WeCare Project, Aerospace, 4, https://doi.org/10.3390/aerospace4030034, 2017a.

Grewe, V., Tsati, E., Mertens, M., Frömming, C., and Jöckel, P.: Contribution of emissions to concentrations: the TAGGING 1.0 submodel based on the Modular Earth Submodel System (MESSy 2.52), Geoscientific Model Development, 10, 2615–2633, https://doi.org/10.5194/gmd-10-2615-2017, 2017b.

Grewe, V., Matthes, S., and Dahlmann, K.: The contribution of aviation NO_x emissions to climate change: are we ignoring methodological flaws?, Environmental Research Letters, 14, 121 003, https://doi.org/10.1088/1748-9326/ab5dd7, https://doi.org/10.1088%2F1748-9326%2Fab5dd7, 2019.

Irvine, E. A., Hoskins, B. J., Shine, K. P., Lunnon, R. W., and Froemming, C.: Characterizing North Atlantic weather patterns for climate-optimal aircraft routing, Meteorological Applications, 20, 80–93, https://doi.org/10.1002/met.1291, 2013.

Jöckel, P., Kerkweg, A., Pozzer, A., Sander, R., Tost, H., Riede, H., Baumgaertner, A., Gromov, S., and Kern, B.: Development cycle 2 of the Modular Earth Submodel System (MESSy2), Geoscientific Model Development, 3, 717–752, https://doi.org/10.5194/gmd-3-717-2010, 2010.

Jöckel, P., Tost, H., Pozzer, A., Kunze, M., Kirner, O., Brenninkmeijer, C. A. M., Brinkop, S., Cai, D. S., Dyroff, C., Eckstein, J., Frank, F., Garny, H., Gottschaldt, K.-D., Graf, P., Grewe, V., Kerkweg, A., Kern, B., Matthes, S., Mertens, M., Meul, S., Neumaier, M., Nützel, M., Oberländer-Hayn, S., Ruhnke, R., Runde, T., Sander, R., Scharffe, D., and Zahn, A.: Earth System Chemistry integrated Modelling (ESCiMo) with the Modular Earth Submodel System (MESSy) version 2.51, Geoscientific Model Development, 9, 1153–1200, https://doi.org/10.5194/gmd-9-1153-2016, 2016.

Kärcher, B.: Formation and radiative forcing of contrail cirrus, Nature Communications, 9, 1824, https://doi.org/10.1038/s41467-018-04068-0, 2018.

Köhler, M., Rädel, G., Shine, K., Rogers, H., and Pyle, J.: Latitudinal variation of the effect of aviation NO_x emissions on atmospheric ozone and methane and related climate metrics, Atmospheric Environment, 64, 1 – 9, https://doi.org/https://doi.org/10.1016/j.atmosenv.2012.09.013, 2013.

Köhler, M. O., Rädel, G., Dessens, O., Shine, K. P., Rogers, H. L., Wild, O., and Pyle, J. A.: Impact of perturbations to nitrogen oxide emissions from global aviation, Journal of Geophysical Research: Atmospheres, 113, https://doi.org/10.1029/2007JD009140, 2008.

Lee, D. S., Fahey, D. W., Forster, P. M., Newton, P. J., Wit, R. C., Lim, L. L., Owen, B., and Sausen, R.: Aviation and global climate change in the 21st century, Atmospheric Environment, 43, 3520 – 3537, https://doi.org/https://doi.org/10.1016/j.atmosenv.2009.04.024, 2009.

Lelieveld, J., Peters, W., Dentener, F. J., and Krol, M. C.: Stability of tropospheric hydroxyl chemistry, Journal of Geophysical Research: Atmospheres, 107, ACH 17–1–ACH 17–11, https://doi.org/10.1029/2002JD002272, https://agupubs.onlinelibrary.wiley.com/doi/abs/10.1029/2002JD002272, 2002.

Lelieveld, J., Gromov, S., Pozzer, A., and Taraborrelli, D.: Global tropospheric hydroxyl distribution, budget and reactivity, Atmospheric Chemistry and Physics, 16, 12 477–12 493, https://doi.org/10.5194/acp-16-12477-2016, 2016.

Matthes, S.: Climate-optimised flight planning–REACT4C in Innovation for a Sustainable Avation in a Global Environment, Proceedings of the Sixth European Aeronautics Days, 2011.

Matthes, S., Schumann, U., Grewe, V., Frömming, C., Dahlmann, K., Koch, A., and Mannstein, H.: Climate Optimized Air Transport, pp. 727–746, Springer Berlin Heidelberg, Berlin, Heidelberg, https://doi.org/10.1007/978-3-642-30183-4_44, 2012.

Mertens, M., Grewe, V., Rieger, V. S., and Jöckel, P.: Revisiting the contribution of land transport and shipping emissions to tropospheric ozone, Atmospheric Chemistry and Physics, 18, 5567–5588, https://doi.org/10.5194/acp-18-5567-2018, 2018.

Orbe, C., Yang, H., Waugh, D. W., Zeng, G., Morgenstern, O., Kinnison, D. E., Lamarque, J.-F., Tilmes, S., Plummer, D. A., Scinocca, J. F., Josse, B., Marecal, V., Jöckel, P., Oman, L. D., Strahan, S. E., Deushi, M., Tanaka, T. Y., Yoshida, K., Akiyoshi, H., Yamashita, Y., Stenke, A., Revell, L., Sukhodolov, T., Rozanov, E., Pitari, G., Visioni, D., Stone, K. A., Schofield, R., and Banerjee, A.: Large-scale tropospheric transport in the Chemistry–Climate Model Initiative (CCMI) simulations, Atmospheric Chemistry and Physics, 18, 7217–7235, https://doi.org/10.5194/acp-18-7217-2018, 2018.

Reithmeier, C. and Sausen, R.: ATTILA: atmospheric tracer transport in a Lagrangian model, Tellus B, 54, 278–299, https://doi.org/10.1034/j.1600-0889.2002.01236.x, 2002.

Riede, H., Jöckel, P., and Sander, R.: Quantifying atmospheric transport, chemistry, and mixing using a new trajectory-box model and a global atmospheric-chemistry GCM, Geoscientific Model Development, 2, 267–280, https://doi.org/10.5194/gmd-2-267-2009, https://www.geosci-model-dev.net/2/267/2009/, 2009.

Roeckner, E., Bäuml, G., Bonaventura, L., Brokopf, R., Esch, M., Giorgetta, M., Hagemann, S., Kirchner, I., Kornblueh, L., Manzini, E., Rhodin, A., Schlese, U., Schulzweida, U., and Tompkins, A.: The atmospheric general circulation model ECHAM 5. Part I: Model description., Tech. Rep. 349, Max-Planck-Institute for Meteorology, Hamburg, 2003.

Sander, R., Kerkweg, A., Jöckel, P., and Lelieveld, J.: Technical note: The new comprehensive atmospheric chemistry module MECCA, Atmospheric Chemistry and Physics, 5, 445–450, https://doi.org/10.5194/acp-5-445-2005, 2005.

Shine, K. P., Derwent, R., Wuebbles, D., and Morcrette, J.: Radiative forcing of climate, in: Climate Change: The IPCC Scientific Assessment (1990), Report prepared for Intergovernmental Panel on Climate Change by Working Group I, edited by Houghton, J. T., Jenkins, G. J., and Ephraums, J. J., chap. 2, pp. 41–68, Cambridge University Press, Cambridge, Great Britain, New York, NY, USA and Melbourne, Australia, 1990.

Stevenson, D. S. and Derwent, R. G.: Does the location of aircraft nitrogen oxide emissions affect their climate impact?, Geophysical Research Letters, 36, https://doi.org/10.1029/2009GL039422, 2009.

Stevenson, D. S., Doherty, R. M., Sanderson, M. G., Collins, W. J., Johnson, C. E., and Derwent, R. G.: Radiative forcing from aircraft NO_x emissions: Mechanisms and seasonal dependence, Journal of Geophysical Research: Atmospheres, 109, https://doi.org/10.1029/2004JD004759, 2004.

Søvde, O. A., Matthes, S., Skowron, A., Iachetti, D., Lim, L., Owen, B., Øivind Hodnebrog, Genova, G. D., Pitari, G., Lee, D. S., Myhre, G., and Isaksen, I. S.: Aircraft emission mitigation by changing route altitude: A multi-model estimate of aircraft NO_x emission impact on O_3 photochemistry, Atmospheric Environment, 95, 468 – 479, https://doi.org/https://doi.org/10.1016/j.atmosenv.2014.06.049, 2014.

van Manen, J. and Grewe, V.: Algorithmic climate change functions for the use in eco-efficient flight planning, Transportation Research Part D: Transport and Environment, 67, 388 – 405, https://doi.org/https://doi.org/10.1016/j.trd.2018.12.016, http://www.sciencedirect.com/science/article/pii/S1361920917309781, 2019.

Wauben, W., Velthoven, P., and Kelder, H.: A 3D chemistry transport model study of changes in atmospheric ozone due to aircraft NO_x emissions, Atmospheric Environment, 31, 1819 – 1836, https://doi.org/https://doi.org/10.1016/S1352-2310(96)00332-9, 1997.

Wild, O., Prather, M. J., and Akimoto, H.: Indirect long-term global radiative cooling from NO_x Emissions, Geophysical Research Letters, 28, 1719–1722, https://doi.org/10.1029/2000GL012573, 2001.

Yin, F., Grewe, V., van Manen, J., Matthes, S., Yamashita, H., Linke, F., and Lührs, B.: Verification of the ozone algorithmic climate change functions for predicting the short-term NOx effects from aviation en-route, in: Proc. of the 8th International Conference for Research in Air Transportation, pp. 1–8, Barcelona, Spain, 2018.